Published in final edited form as:

Nat Geosci. 2016 December ; 9(12): 875–879. doi:10.1038/NGEO2827.

Tropospheric ozone change from 1980 to 2010 dominated by equatorward redistribution of emissions

Yuqiang Zhang[1,2], **Owen R. Cooper**[3,4], **Audrey Gaudel**[3,4], **Philippe Nédélec**[5], **Shin-Ya Ogino**[6], **Anne M. Thompson**[7], **J. Jason West**[1]

[1]Environmental Sciences and Engineering Department, University of North Carolina at Chapel Hill, Chapel Hill, NC 27599, USA

[3]Cooperative Institute for Research in Environmental Sciences, University of Colorado, Boulder, CO 80309, USA

[4]Chemical Sciences Division, NOAA Earth System Research Laboratory, Boulder, CO 80305, USA

[5]Laboratoire d'Aérologie, CNRS, Université Paul Sabatier Toulouse III, FR-31062 Toulouse, France

[6]Japan Agency for Marine-Earth Science and Technology, Yokosuka 237-0061, Japan

[7]NASA Goddard Space Flight Center, Greenbelt, MD 20771, USA

Abstract

Since 1980, anthropogenic emissions of ozone precursors have decreased in developed regions, but increased in developing regions, particularly East and South Asia, redistributing emissions equatorwards[1–4]. Modeling studies have shown that the tropospheric ozone burden (B_{O3}) is much more sensitive to emission changes in the tropics and Southern Hemisphere (SH) than other regions[5–9]. However, the effect of the spatial redistribution of emissions has not been isolated. Here we use a global chemical transport model to consider changes in anthropogenic short-lived emissions from 1980 to 2010, and separate the influence of changes in the spatial distribution of emissions from the total emission increase, on B_{O3} and surface ozone. We estimate that the spatial distribution change increased B_{O3} by slightly more than the combined influences of changes in the global emission magnitude itself and in global methane. These results are explained by the strong convection, fast reaction rates, and strong NO_x sensitivity in the tropics and subtropics. Emissions increases in Southeast, East, and South Asia may be most important for the B_{O3} change. The spatial distribution of emissions has a dominant effect on global tropospheric ozone, suggesting

[2]now at Environmental Protection Agency, Research Triangle Park, NC 27709, USA.

Author contributions

Y.Q.Z., J.J.W., and O.R.C. designed the study and Y.Q.Z. and J.J.W. planned the model experiments. Y.Q.Z. prepared the emission inputs, performed the model simulations, and prepared the figures. Y.Q.Z. and A.G. conducted data analysis for observations, and J.J.W. and O.R.C. assisted with the data analysis. P.N., S.-Y.O., and A.M.T. provided observational data. Y.Q.Z., J.J.W. and O.R.C. wrote the paper with comments from A.M.T and A.G.

Competing financial interests

The authors declare no competing financial interests.

that the future ozone burden will be determined mainly by emissions from the tropics and subtropics.

Ozone (O_3) at the surface is an important air pollutant, detrimental to human health and crop yield[10]; in the troposphere, O_3 is the third most important anthropogenic greenhouse gas[11]. O_3 production in the troposphere, by the oxidation of carbon monoxide (CO), non-methane volatile organic compounds (NMVOCs), and methane (CH_4) in the presence of nitrogen oxides (NO_x) and sunlight, exceeds the stratosphere-to-troposphere exchange by a factor of 5–7 (ref. 12). O_3 is an urban and regional air pollutant, but is also sufficiently long lived (~ 22 days globally averaged[12]) that its baseline concentrations are elevated over the entire Northern Hemisphere (NH) (ref. 13). Observations[14] and models[15,16] have associated emission increases in Asia with increasing O_3 above western North America. The tropospheric O_3 burden (B_{O3}) is an important quantity that is related to radiative forcing (RF), as O_3 is more effective as a greenhouse gas in the middle and upper troposphere than near the surface[11], and to surface air quality because it influences both urban and rural baseline ozone.

From 1940 to 1980, global anthropogenic emissions of O_3 precursors increased, but the spatial distribution remained fairly unchanged, with the greatest emissions in the NH middle and high latitudes. Starting in 1980, emissions began to shift equatorward as China and low-latitude nations became more industrialized. From 1980 to 2010, global anthropogenic emissions of CO, NO_x, and NMVOCs are estimated to have increased by 6.4%, 21.2%, and 6.0% (refs 3,17), and the global CH_4 mixing ratio increased by 14.7% (231 ppbv, ref. 18). During the same period, emissions of CO and NMVOCs increased south of 30°N but decreased north of this latitude, while NO_x emissions increased south of 40°N but decreased to the north (Supplementary Figs. 1 and 2).

Here we investigate the influences of global emission changes from 1980 to 2010 on B_{O3} and surface O_3, separating the influences of changes in: (i.) the spatial distribution of anthropogenic short-lived emissions; (ii.) the global magnitude of emissions; and (iii.) the global CH_4 mixing ratio. Simulations are conducted with the CAM-chem[19] global chemical transport model for 1980 and 2010, and sensitivity simulations alter these three parameters individually to 1980 conditions, relative to the 2010 simulation (Methods; Supplementary Table 1).

The global B_{O3} is modeled to have increased by 28.12 Tg (8.9%) from 1980 to 2010 (four-year averages), with 57% of the total increase in the NH (Fig. 1). The largest B_{O3} increases are over 30°S–30°N (17.93 Tg, Figs. 1 and 2). The influence of the change in the spatial distribution of global anthropogenic emissions contributes 16.39 Tg of the total tropospheric O_3 burden change (ΔB_{O3}), also higher in the NH than in the SH, slightly greater than the combined influences of the change in emission magnitude (8.59 Tg) and the global CH_4 change (7.48 Tg) (Fig. 2). The influence of the change in spatial distribution is greater than the sum of the other two influences in three of four years modeled, with the interannual variability in ΔB_{O3} being much smaller than the overall change (Supplementary Table 2). The sensitivity of B_{O3} to CH_4 here (0.123 Tg B_{O3} per Tg CH_4 a^{-1}) is within the range of other models (0.11–0.16 Tg B_{O3} per Tg CH_4 a^{-1}, ref. 20). Note that the total ΔB_{O3} from the

sum of the three sensitivity simulations (32.46 Tg) is larger than the difference between S_2010 (Supplementary Table 1) and S_1980 (28.12 Tg), as only one variable is changed to 1980 conditions in each simulation. Over 30°S–30°N, the ΔB_{O_3} from the emission spatial distribution change is much greater than the other influences. In extratropical regions, the ΔB_{O_3} from the emission spatial distribution change is only slightly greater or comparable to ΔB_{O_3} from the other two. North of 60°N, the ΔB_{O_3} due to the emission spatial distribution change is lowest, as less O_3 and its precursors are transported from North America and Europe.

Between 1980 and 2010, the greatest modeled increases in O_3 burden are over 10°–35°N from the surface to the upper troposphere (Fig. 3). 68% of ΔB_{O_3} occurs below 500 hPa, although the greatest changes in mixing ratio are in the middle and upper troposphere (Supplementary Fig. 4). Notable O_3 increases are also seen over 30°S–10°N. Over 35°–60°N, O_3 increases at all altitudes, even though anthropogenic emissions from North America and Europe decreased between 1980 and 2010 (Supplementary Figs. 1 and 2). The influences of the global emission magnitude change and the global CH_4 change both increase O_3 over 30°S–35°N, but the emission spatial distribution change best explains the overall O_3 change, particularly the regions with greatest ozone increases. Increases in O_3 precursor emissions South of 35°N are transported efficiently to the middle and upper troposphere, from strong convection in the Hadley cell, whereas emission decreases North of 35°N stay at high latitudes and low elevation in Ferrell cell circulation (Fig. 4). When global emissions shift equatorward, strong convective mixing over the tropics and subtropics lifts O_3 and its precursor NO_y to higher altitudes (Figs. 3b, 4b, Supplementary Fig. 6), where the O_3 lifetime is longer, favoring O_3 accumulation. When emission increases occur in NH mid-latitudes, less NO_y is lofted to high altitudes (Fig. 4c). O_3 increases at high altitudes over middle and high latitudes are affected by the transport of pollutants from the tropics and subtropics[16,21] (Fig. 3b).

In addition to strong convection, the tropics and subtropics have faster chemical reaction rates than other regions (Supplementary Fig. 8), due to the strong sunlight and warm temperatures. Therefore changes in the O_3 chemical production (P_{O3}), and loss (L_{O3}) rates are greater for the spatial distribution change than for the magnitude change, due to greater low-latitude emissions (Supplementary Fig. 9). Similarly, the distribution change increases the global ozone production efficiency, whereas the magnitude change decreases it. In addition, strong NO_x-sensitivity prevails over the tropics and subtropics, especially in the middle and upper troposphere (Supplementary Figs 10 and 11), and emission trends show greater increases of NO_x than of NMVOCs (Supplementary Fig. 1). Finally, O_3 lifetime is lower over the tropics, due to destruction from water vapor and dry deposition to vegetated surfaces[21]. However, this effect is clearly not dominant as we see larger O_3 increases over the tropics.

In Fig. 2, the largest modeled ΔB_{O_3} occurs over South and Southeast Asia, suggesting a strong influence of emission increases in these regions. We estimate the importance of different regions for B_{O3} by multiplying the change in NO_x emissions in each of nine world regions by the sensitivity of B_{O3} per unit NO_x emissions from West et al.[7] (Supplementary Table 3). Doing so, we find that emissions changes from Southeast Asia are most important

for the 1980–2010 global ΔB_{O3}, followed by East Asia and South Asia. Southeast Asia emerges as most important – although its emission increase is roughly 1/5 that from East Asia – because of the very large sensitivity of B_{O3} to NO_x emissions. Strong convection over Southeast Asia contributes to this large sensitivity, and convection over the Himalayas in the NH summer, when the intertropical convergence zone is farthest north, also suggest a pathway for South Asian emissions to the upper troposphere[21] (Supplementary Figs. 6, 7). Future work should model the contributions of emissions changes from each region individually.

Surface O_3 changes, using the three month O_3-season Maximum Daily 8-hr Average O_3 (MDA8) (Supplementary Fig. 12), are dominated by regional emission trends: decreases within Europe and North America, and increases over East Asia and Southeast Asia, consistent with observations[10,22]. Similar regional variations of MDA8 O_3 are also seen from the influence of the global emission spatial pattern change. The MDA8 change between 1980 and 2010 is therefore also dominated by the global emission spatial pattern change, with smaller contributions from the global emission magnitude and CH_4 changes.

These modeled ozone changes are broadly consistent with observed changes over recent decades that show strong increases in South, East, and Southeast Asia (Supplementary Information)[22]. Comparing S_1980 with the global ozonesonde climatology of Logan et al.[23], and S_2010 with that of Tilmes et al.[24] (Supplementary Figs. 13 and 14), the model compares well in both time periods, but is biased high at 200 mb in S_1980 between 30°S and the equator, and that bias increases in S_2010 between 30°S and 30°N. At NH-midlatitude long-term ozonesonde sites, the model overestmates the 1980–2010 ozone change at two of three sites (Supplementary Fig. 15). However, IAGOS commercial aircraft[25] and SHADOZ ozonesondes[26] in Southeast Asia, northeastern China, and southern India show good agreement with the model, and for the first time show statistically significant ozone increases at most elevations from 1994–2004 to 2005–2014, which are similar to the modeled 1980–2010 changes (Supplementary Figs. 16–18). Compared with six long-term rural or remote surface sites, the model captures well the 1980–2010 O_3 trend at five sites, though tending to overestimate the trend, and it overestimates O_3 in the NH and underestimates in the SH (Supplementary Fig. 19). Compared with OMI/MLS satellite observations[27], the S_2010 modeled B_{O3} has high biases, particularly in the tropics and subtropics including over Africa (Supplementary Fig. 20), that are comparable to the simulated 1980–2010 burden change (Supplementary Tables 7, 8), and thus the model may overstate the magnitude of the tropical and subtropical ozone changes. However, OMI/MLS trends in ozone columns from 2004 to 2015 show the greatest growth over South and Southeast Asia (Supplementary Fig. 21), consistent with the model (Fig. 2). Despite model biases, these observations provide strong evidence for ozone increases in these regions that are generally consistent with the model.

Observations have also shown that the ozone peak has shifted earlier in the year at rural NH sites, and emissions moving equatorward has been hypothesized as an eplanation[22,288]. However, S_2010 does not show the observed shift in the timing of ozone peaks relative to S_1980, nor does S_Distribution (Supplementary Fig. 22). Uncertainty in historical

emissions and seasonal distributions, or inaccuracies in model chemistry or physics[29], may be the reasons for our inability to explain these observations.

We use a single global chemical transport model, and results with other models may differ, particularly due to different reaction mechanisms. We evaluate the contributions of each parameter by simulating 1980 conditions for each parameter individually, relative to the 2010 simulation, and ΔB_{O_3} would likely be smaller had we evaluated relative to 1980. However, we expect that the relative contributions would be similar. By using the same meteorology in 1980 and 2010, we neglect the possible effects of climate change or climate variability on ΔB_{O_3}.

These results are expected to have important implications for the RF of O_3. However, increasing NO_x may cause a negative RF, due mainly to decreases in CH_4, and regions with high sensitivity of B_{O3} to NO_x emissions also have a high sensitivity of CH_4 to NO_x, with the two RFs roughly canceling over all source regions[5,8]. CO is sufficiently long-lived that the sensitivity of B_{O3} does not vary strongly with the location of CO emissions[30]. The effect of the equatorward emission shift on RF should be investigated further.

The change in the spatial distribution of the global anthropogenic emissions from 1980 to 2010 dominates the B_{O3} change, slightly greater than the combined effects of changes in the global emission magnitude and global CH_4. In particular, increases in O_3 precursor emissions in the tropics and subtropics significantly influence the global B_{O3}, and our findings suggest that emissions increases from Southeast, East, and South Asia have been most important for the B_{O3} increase. This can be attributed to the strong photochemical reaction rates, convection, and NO_x-sensitivity in the tropics and subtropics. These findings suggest that scientific and policy analyses should put a greater emphasis on emission location and the dominant role of emissions from the tropics and subtropics for B_{O3}. As a result, the global B_{O3} might continue to increase due to a continued equatorward shift of emissions, even if global anthropogenic emissions remain unchanged or even decrease.

Methods

Global emissions spatial pattern change

Here we use anthropogenic emissions including biomass burning in 1980 from the Atmospheric Chemistry and Climate Model Intercomparison Project (ACCMIP, ref. 3), and in 2010 from the Representative Concentration Pathways 8.5 (RCP8.5) scenario[17,31], which are downloaded from the RCP database (http://tntcat.iiasa.ac.at:8787/RcpDb/dsd?Action=htmlpage&page=download, accessed 10/31/2014) to analyze emission trends and drive the global model (Supplementary Figs 1 and 2). RCP8.5 2010 emissions are self-consistent with the ACCMIP historical emissions, and are considered to be the most reasonable scenario to extend ACCMIP emissions beyond 2000 (ref. 4) as they track the GAINS current legislation scenario for several decades[17]. The 2010 global total anthropogenic emissions of CO, NO_x and NMVOCs are 1030 Tg, 82 Tg NO, and 180 Tg, respectively. As with other global emission estimates for short-lived species, emissions are uncertain and may be especially uncertain in some developing regions[29,32–34]. The rapid growth of emissions in the tropics and subtropics is seen in global emission inventories[3,4] as

well as regional ones[35,36]. These inventories are supported by observations from satellites[1,2,37,38] and from surface and airborne observations[29,39] that show that NO_2 in developed regions, such as Europe and North America, have greatly diminished emissions since 1980, but the emissions are increasing in developing countries, especially China and India, shifting global emissions equatorward.

CAM-chem model configuration

We use the global chemistry-climate model CAM-chem, which is based on the global Community Atmosphere Model (CAM) version 4, the atmospheric component of the Community Earth System Model (CESM, v1.2.2) (refs 19,40). The model has a horizontal resolution of 1.9° (latitude) × 2.5° (longitude), and 56 vertical levels between the surface and 4 hPa (≈40 km) with a time step of 1800 s. We use the NASA Global Modeling and Assimilation Office GEOS-5 meteorology to drive the model as a chemical transport model. For all simulations, we run CAM-chem for five consecutive years, with the first-year as spin-up and results are shown as a four-year average. Monthly-mean distributions of chemically-active stratospheric species (such as O_3, NO, NO_2 and N_2O_5) are prescribed using the climatology from the Whole Atmospheric Community Climate Model (WACCM) simulations[41], following Lamarque et al.[19].

Non-methane volatile organic compound (NMVOCs) species from ACCMIP (1980) and RCP8.5 (2010) are both re-speciated to match the CAM-chem VOC categories following previous studies[30,42,43]. Monthly temporal variations for all anthropogenic emissions sectors are also added based on the monthly time-dependence of emissions from RETRO[30,42–44], except for aircraft, shipping and biomass burning for which seasonal variations were provided. The Model of Emissions of Gases and Aerosols from Nature (MEGAN-v2.1, ref. 45) simulates biogenic emissions for 150 compounds online within CAM-chem, yielding four-year average global biogenic emissions of isoprene, monoterpene, methanol and acetone of 420.69 Tg yr^{-1}, 133.23 Tg yr^{-1}, 91.99 Tg yr^{-1} and 42.67 Tg yr^{-1}. Lightning NO_x emissions are calculated online as 3.21 TgN yr^{-1} (four-year average); this is lower than the average of ACCMIP models for 2000, but within the range[12], which may affect the sensitivity of ozone to NO_x and VOCs, particularly in the tropics and mid-troposphere where lightning emissions are greatest. Other natural emissions (ocean, volcano and soil) are from the standard CAM-chem emission files (for 2000), and remain the same for all the simulations, with soil NO_x at 8.0 TgN yr^{-1} (refs 19,46). The CH_4 volume mixing ratio (ppb) is fixed at uniform global values of 1567 and 1798 ppbv for 1980 and 2010 (ref. 18).

In addition to simulating 1980 and 2010, we conduct three sensitivity simulations in which the spatial distribution of global anthropogenic emissions (S_Distribution), the magnitude of the global emissions (S_Magnitude), and the global CH_4 mixing ratio (S_CH_4) are individually set to 1980 levels and all other parameters stay the same as the 2010 simulation (Supplementary Table 1). Here global anthropogenic emissions refer to all short-lived species, including ozone precursors and other species such as aerosols, from anthropogenic sources including biomass burning. The differences between S_2010 and S_1980 reflect the total emission changes from 1980 to 2010. Each of the other three simulations is subtracted from S_2010 to isolate individual influences. We use meteorology from 2009–2012 with

2008 as a spin-up for all simulations, isolating the effects of changes in emissions and neglecting possible effects of climate variability or change from 1980 to 2010.

Tropospheric O_3 burden (B_{O3}) is defined as the total below the chemical tropopause of 150 ppbv ozone in the S_2010 simulation, with the same tropopause applied to all simulations. The four-year average B_{O3} in S_2010 is 342.7 Tg, within the range of ACCMIP models (337±23 Tg for 1995–2005), and the 1980–2010 ΔB_{O_3} of 28.12 Tg is similar to the ACCMIP 15±6 Tg for 1980–2000, and 41±12 for 1980–2030 (RCP8.5) (ref. 12). The three-month ozone season average MDA8 is found for the consecutive three-month period with the highest MDA8 in each grid cell. NO_y (total reactive nitrogen) is calculated as NO + NO_2 + NO_3 + HNO_3 + HO_2NO_2 + 2×N_2O_5 + $CH_3CO_3NO_2$ (PAN) + $CH_2CCH_3CO_3NO_2$ (MPAN, methacryloyl peroxynitrate) + $CH_2CHCCH_3OOCH_2ONO_2$ ($ISOPNO_3$, peroxy radical from NO_3+ isoprene) from CAM-chem output.

CAM-chem evaluation

A comprehensive evaluation of the CAM-chem 2010 simulation is performed using a present-day climatology of O_3 data from multi-year observations from ozonesondes, satellites, aircraft campaigns, and ground-based observations, compared with the four-year average of CAM-chem output. Our model captures the vertical distribution of O_3 in ozonesondes[24] very well, though it is biased high between 30°S and 30°N, particularly in the upper troposphere (Supplementary Table 4; Supplementary Fig. 23). The seasonal cycles of O_3 at specific pressure levels from the ozonesonde data are also captured well by the model (Supplementary Fig. 24), with a correlation coefficient between the observed and simulated monthly regional O_3 average that is usually greater than 0.8 (Supplementary Fig. 25). When evaluating the model performance with aircraft campaign observations, we focus on the regional average over the campaign areas, and analyze the data at different altitudes. Generally, the model performs better in the NH than the SH (Supplementary Fig. 26). When evaluated with multi-year satellite data[27], the model overestimates O_3 between 20°S and 40°N, and overestimations in this region are common for global models[12], with a modeled global B_{O3} that is 23.8 Tg higher (Supplementary Fig. 20). Compared with surface O_3 observations, S_2010 overestimates O_3 by 5.75 ppbv averaged over all stations in the US (Supplementary Fig. 27), and 0.65 ppbv over Europe (Supplementary Fig. 28), but captures well the seasonal cycles.

Data sources

Hourly O_3 observations for the remote sites of Barrow, Mauna Loa, Samoa and South Pole are maintained by the NOAA Global Monitoring Division (GMD) and can be found here: ftp://aftp.cmdl.noaa.gov/data/ozwv/SurfaceOzone/

Hourly ozone data from Hohenpeissenberg for the years 1971–2010 were downloaded from the Global Atmosphere Watch (GAW) World Data Centre for Greenhouse

Gases: http://ds.data.jma.go.jp/gmd/wdcgg. The Meteorological Observatory Hohenpeissenberg is operated and financed by the German Meteorological Service (DWD).

The Whiteface Mountain Summit ozone data were collected by the University at Albany-SUNY with instrumentation provided by the New York State Department of Environmental Conservation. The data set was provided by James J. Schwab, Atmospheric Sciences Research Center, University at Albany-SUNY. These data are also archived by the United States Environmental Protection Agency: http://www.epa.gov/ttn/airs/aqsdatamart.

Monthly OMI/MLS tropospheric column ozone data (Ziemke et al., 2011) were provided by Jerald Ziemke, Morgan State University, Baltimore, and downloaded from: http://acd-ext.gsfc.nasa.gov/Data_services/cloud_slice/. The OMI/MLS tropospheric column ozone product, is derived from the Ozone Monitoring Instrument (OMI) and Microwave Limb Sounder (MLS) remote sensors onboard NASA's polar orbiting Aura satellite. MLS retrievals are the latest available, version 4.2.

Ozone profiles from commercial aircraft were collected and made freely available by the Measurement of Ozone and water vapour on Airbus In-service airCraft – In-service Aircraft for a Global Observing System (MOZAIC-IAGOS) programme (www.iagos.org). The data were made possible by: the European Commission's support for the MOZAIC project (1994–2003) and the preparatory phase of IAGOS (2005–2012); the partner institutions of the IAGOS Research Infrastructure (FZJ, DLR, MPI, KIT in Germany, CNRS, CNES, Météo-France in France and University of Manchester in United Kingdom); ETHER (CNES-CNRS/INSU) for hosting the database; and the participating airlines (Lufthansa, Air France, Austrian, China Airlines, Iberia, Cathay Pacific) for the transport free of charge of the instrumentation. The Hanoi, Vietnam ozonesondes were made freely available by the NASA Southern Hemisphere ADditional OZonesondes (SHADOZ) project (Thompson et al., 2007). Observations were made possible by: Mr. Hoang Gia Hiep, Director of the Aero-Meteorological Observatory (AMO), National Hydro-Meteorological Service (NHMS) of S.R. Vietnam; Masato Shiotani, Research Institute for Sustainable Humanosphere (RISH) Kyoto University, Japan. The processed ozonesonde climatology of Logan et al.[23] was shared by Paul Young of Lancaster University.

Code availability

The CAM-chem model code used to perform all the simulations is available here: https://www2.cesm.ucar.edu/models.

The diagnostic package used to perform the model evaluation is developed and maintained by the NCAR AMWG, and code can be found here: https://www2.cesm.ucar.edu/working-groups/amwg/amwg-diagnostics-package/find-code.

Supplementary Material

Refer to Web version on PubMed Central for supplementary material.

Acknowledgments

Y.Q.Z. and J.J.W. were funded by National Institute of Environmental Health Sciences grant #1 R21 ES022600-01 and Environmental Protection Agency STAR grant #834285, and O.R.C was funded by NOAA's Health of the Atmosphere and Atmospheric Chemistry and Climate Programs. We thank the NCAR AMWG for developing and maintaining the diagnostic package for the model evaluation. We acknowledge the free use of O_3 observation data

from NOAA GMD for the remote sites of Barrow, Mauna Loa, Samoa and South Pole; Global Atmosphere Watch World Data Centre for Greenhouse Gases for Hohenpeissenberg, and Dr. Jim Schwab from University at Albany-SUNY for Whiteface Mountain.

References

1. Richter A, Burrows JP, Nüss H, Granier C, Niemeier U. Increase in tropospheric nitrogen dioxide over China observed from space. Nature. 437:129–132.2005; [PubMed: 16136141]
2. Duncan BN, et al. A space-based, high-resolution view of notable changes in urban NOx pollution around the world (2005–2014). J. Geophys. Res. 121:976–996. D024121.2016;
3. Lamarque JF, et al. Historical (1850–2000) gridded anthropogenic and biomass burning emissions of reactive gases and aerosols: Methodology and application. Atmos. Chem. Phys. 10:7017–7039.2010;
4. Granier C, et al. Evolution of anthropogenic and biomass burning emissions of air pollutants at global and regional scales during the 1980–2010 period. Clim. Change. 109:163–190.2011;
5. Naik V, et al. Net radiative forcing due to changes in regional emissions of tropospheric ozone precursors. J. Geophys. Res. Atmos. 110:D24306.2005;
6. Derwent RG, et al. Radiative forcing from surface NO_x emissions: spatial and seasonal variations. Clim. Change. 88:385–401.2008;
7. West JJ, Naik V, Horowitz LW, Fiore AM. Effect of regional precursor emission controls on long-range ozone transport – Part 1: Short-term changes in ozone air quality. Atmos. Chem. Phys. 9:6077–6093.2009;
8. Fry MM, et al. The influence of ozone precursor emissions from four world regions on tropospheric composition and radiative climate forcing. J. Geophys. Res. Atmos. 117:D07306.2012;
9. Gupta ML, Cicerone RJ, Elliott S. Perturbation to global tropospheric oxidizing capacity due to latitudinal redistribution of surface sources of NO_x, CH_4 and CO. Geophys. Res. Lett. 25:3931–3934.1998;
10. The Royal Society. Ground-level ozone in the 21st century: future trends, impacts and policy implications. The Royal Society Science Policy; London SW1Y 5AG, UK: 2008.
11. Myhre, G, , et al. Climate Change 2013: The Physical Science Basis. Contribution of Working Group I to the Fifth Assessment Report of the Intergovernmental Panel on Climate Change Ch. 8. Cambridge Univ. Press; Cambridge, United Kingdom and New York, NY, USA: 2013.
12. Young PJ, et al. Pre-industrial to end 21st century projections of tropospheric ozone from the Atmospheric Chemistry and Climate Model Intercomparison Project (ACCMIP). Atmos. Chem. Phys. 13:2063–2090.2013;
13. Hemispheric Transport of Air Pollution 2010—Part A Ozone and Particulate Matter. United Nations Economic Commission for Europe; Geneva: 2010.
14. Cooper OR, Gao R-S, Tarasick D, Leblanc T, Sweeney C. Long-term ozone trends at rural ozone monitoring sites across the United States, 1990–2010. J. Geophys. Res. Atmos. 117:D22307.2012;
15. Cooper OR, Andrew O, Parrish DD, Fahey DW. Challenges of a lowered U.S. ozone standard. Science. 348:1096–1097.2015; [PubMed: 26045425]
16. Verstraeten WW, et al. Rapid increases in tropospheric ozone production and export from China. Nat. Geosci. 2015; doi: 10.1038/ngeo2493
17. Riahi K, et al. RCP 8.5-A scenario of comparatively high greenhouse gas emissions. Clim. Change. 109:33–57.2011;
18. Prather, M, , et al. Climate Change 2013: The Physical Science Basis. Contribution of Working Group I to the Fifth Assessment Report of the Intergovernmental Panel on Climate Change Annex II. Cambridge Univ. Press; Cambridge, United Kingdom and New York, NY, USA: 2013.
19. Lamarque J-F, et al. CAM-chem: description and evaluation of interactive atmospheric chemistry in the Community Earth System Model. Geosci. Model Dev. 5:369–411.2012;
20. Fiore AM, West JJ, Horowitz LW, Naik V, Schwarzkopf MD. Characterizing the tropospheric ozone response to methane emission controls and the benefits to climate and air quality. J. Geophys. Res. 113:D08307.2008;

21. Lawrence MG, Rolf von K, Salzmann M, Rasch PJ. The balance of effects of deep convective mixing on tropospheric ozone. Geophys. Res. Lett. 30:3–6.2003;
22. Cooper OR, et al. Global distribution and trends of tropospheric ozone: An observation-based review. Elem. Sci. Anthr. 2:000029.2014;
23. Logan JA. An analysis of ozonesonde data for the troposphere: Recommendations for testing 3-D models and development of a gridded climatology for tropospheric ozone. J. Geophys. Res. 104:16115–16149.1999;
24. Tilmes S, et al. Technical Note: Ozonesonde climatology between 1995 and 2011: Description, evaluation and applications. Atmos. Chem. Phys. 12:7475–7497.2012;
25. Petzold A, et al. Global-scale atmosphere monitoring by in-service aircraft – current achievements and future prospects of the European Research Infrastructure IAGOS. Tellus B. 67:28452.2015;
26. Thompson AM, et al. Southern Hemisphere Additional Ozonesondes (SHADOZ) 1998–2004 tropical ozone climatology: 3. Instrumentation, station-to-station variability, and evaluation with simulated flight profiles. J. Geophys. Res. 112:D03304.2007;
27. Ziemke JR, et al. A global climatology of tropospheric and stratospheric ozone derived from Aura OMI and MLS measurements. Atmos. Chem. Phys. 11:9237–9251.2011;
28. Parrish D, et al. Lower tropospheric ozone at northern midlatitudes: Changing seasonal cycle. Geophys. Res. Lett. 40:1631–1636.2013;
29. Parrish DD, et al. Long-term changes in lower tropospheric baseline ozone concentrations: Comparing chemistry-climate models and observations at northern midlatitudes. J. Geophys. Res. Atmos. 119:719–5736.2014;
30. Fry MM, et al. Net radiative forcing and air quality responses to regional CO emission reductions. Atmos. Chem. Phys. 13:5381–5399.2013;
31. Moss RH, et al. The next generation of scenarios for climate change research and assessment. Nature. 463:747–756.2010; [PubMed: 20148028]
32. Schopp W, Klimont Z, Suutari R, Cofala J. Uncertainty analysis of emissions estimates in the RAINS integrated assessment model. Environ. Sci. Policy. 8(6):601.2005;
33. Bond TC, et al. Historical emissions of black and organic carbon aerosol from energy-related combustion, 1850–2000. Glob. Biogeo. Cycles. 21:GB2018.2007;
34. Smith SJ, et al. Anthropogenic sulfur dioxide emissions: 1850–2005. Atmos. Chem. Phys. 11:1101–1116.2011;
35. Ohara T, et al. An Asian emission inventory of anthropogenic emission sources for the period 1980–2020. Atmos. Chem. Phys. 7:4419–4444.2007;
36. Liousse C, Essamoi E, Criqui P, Granier C, Rosset R. Explosive growth in African combustion emissions from 2005 to 2030. Environ. Res. Lett. 9:035003.2014;
37. van der ARJ, et al. Trends, seasonal variability and dominant NO_x source derived from a ten year record of NO_2 measured from space. J. Geophys. Res. Atmos. 113:D04302.2008;
38. Hilboll A, Richter A, Burrows JP. Long-term changes of tropospheric NO2 over megacities derived from multiple satellite instruments. Atmos. Chem. Phys. 13:4145–4169.2013;
39. Thompson AM, et al. Tropospheric ozone increases over the southern Africa region: bellwether for rapid growth in Southern Hemisphere pollution? Atmos. Chem. Phys. 14:9855–9869.2014;
40. Tilmes S, et al. Description and evaluation of tropospheric chemistry and aerosols in the Community Earth System Model (CESM1.2). Geosci. Model Dev. 8:1395–1426.2015;
41. Garcia RR, Marsh DR, Kinnison DE, Boville BA, Sassi F. Simulation of secular trends in the middle atmosphere, 1950–2003. J. Geophys. Res. Atmos. 112:D09301.2007;
42. Fry MM, Schwarzkopf MD, Adelman Z, West JJ. Air quality and radiative forcing impacts of anthropogenic volatile organic compound emissions from ten world regions. Atmos. Chem. Phys. 14:523–535.2014;
43. West JJ, et al. Co-benefits of Global Greenhouse Gas Mitigation for Future Air Quality and Human Health. Nat. Clim. Chang. 3:885–889.2013; [PubMed: 24926321]
44. Schultz, MG, , et al. REanalysis of the TROpospheric Chemical Composition over the Past 40 Years (RETRO)—A Long-term Global Modeling Study of Tropospheric Chemistry Final Report. Jülich/Hamburg; Germany: Aug, 2007

45. Guenther AB, et al. The model of emissions of gases and aerosols from nature version 2.1 (MEGAN2.1): An extended and updated framework for modeling biogenic emissions. Geosci. Model Dev. 5:1471–1492.2012;

46. Emmons LK, et al. Description and evaluation of the Model for Ozone and Related chemical Tracers, version 4 (MOZART-4). Geosci. Model Dev. 3:43–67.2010;

47. Liu SC, et al. Ozone production in the rural troposphere and the implications for regional and global ozone distributions. J. Geophys. Res. 92:4191–4207.1987;

48. Sillman S, He D, Cardelino C, Imhoff RE. The use of photochemical indicators to evaluate ozone-NO_x-hydrocarbon sensitivity: Case studies from Atlanta, New York, and Los Angeles. J. Air Waste Manag. Assoc. 47:1030–1040.1997; [PubMed: 28445117]

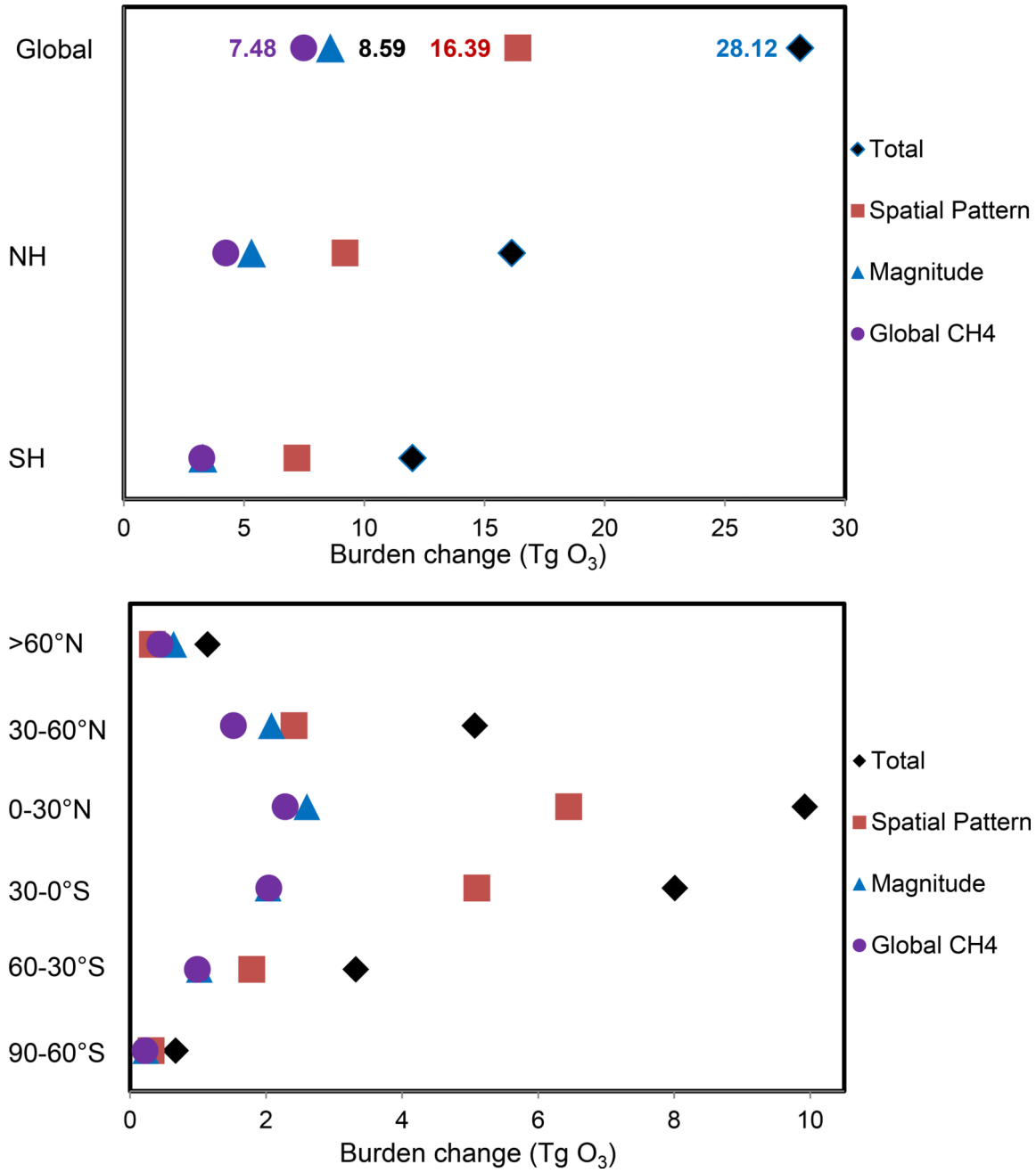

Figure 1. Tropospheric O_3 burden change (ΔB_{O_3}) from 1980 to 2010

ΔB_{O_3} is shown globally, in each hemisphere, and in different latitudinal bands. The estimated components of ΔB_{O_3} due to the emission spatial distribution change (red rectangle), magnitude change (black triangle) and global CH_4 change (purple circle) are also seen.

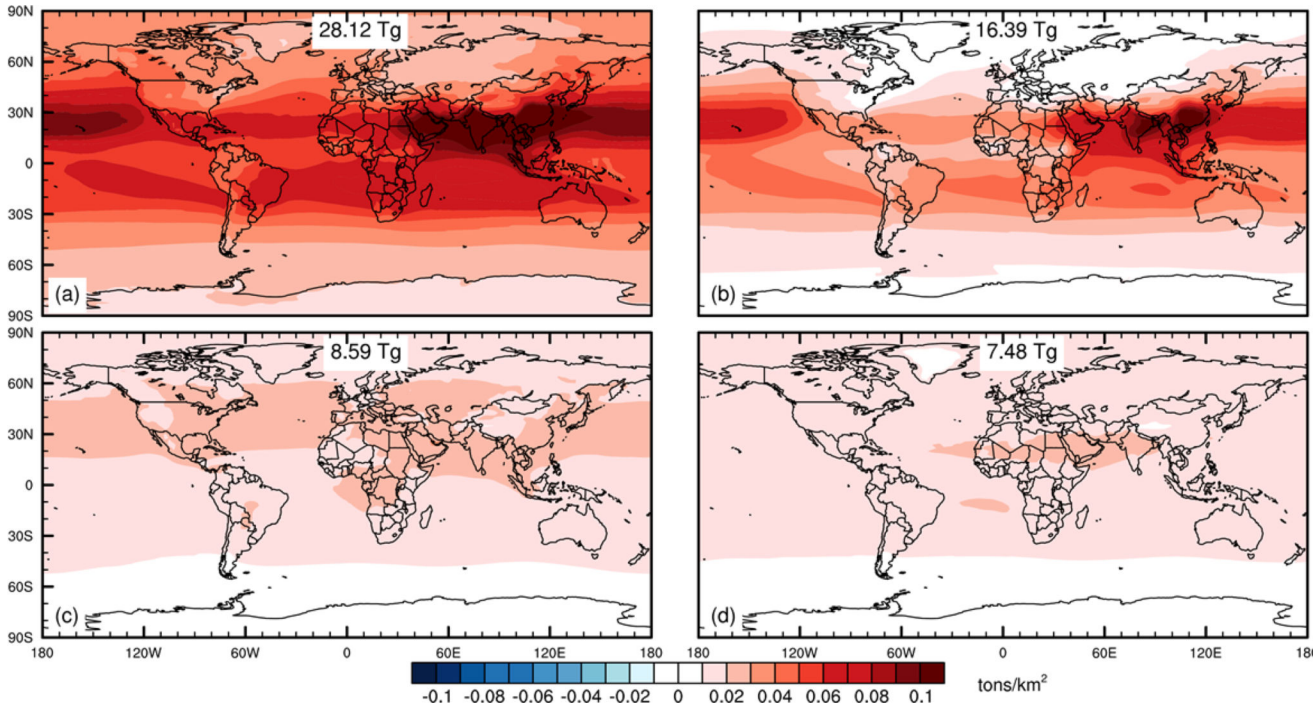

Figure 2. Spatial distributions for ΔB_{O_3} (unit tons/km^2) from 1980 to 2010

a, Total changes from 1980 to 2010. **b-d,** Influences of changes in the global emissions spatial distribution, the global emissions magnitude, and global CH_4 mixing ratio.

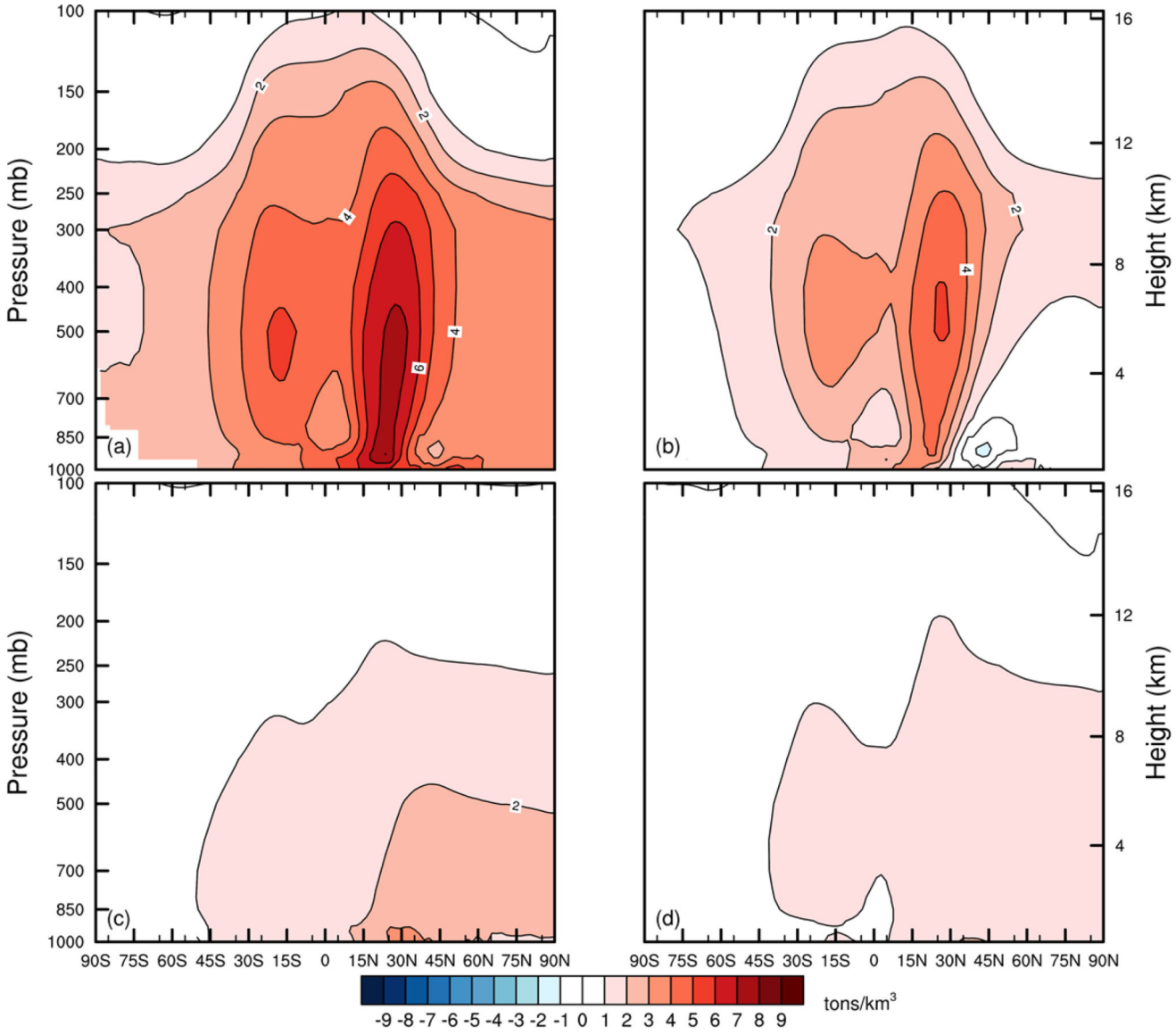

Figure 3. Zonal annual average O_3 change

a, Total change from 1980 to 2010. **b-d,** Influences of changes in the global emissions spatial distribution, the global emissions magnitude, and global CH_4 mixing ratio.

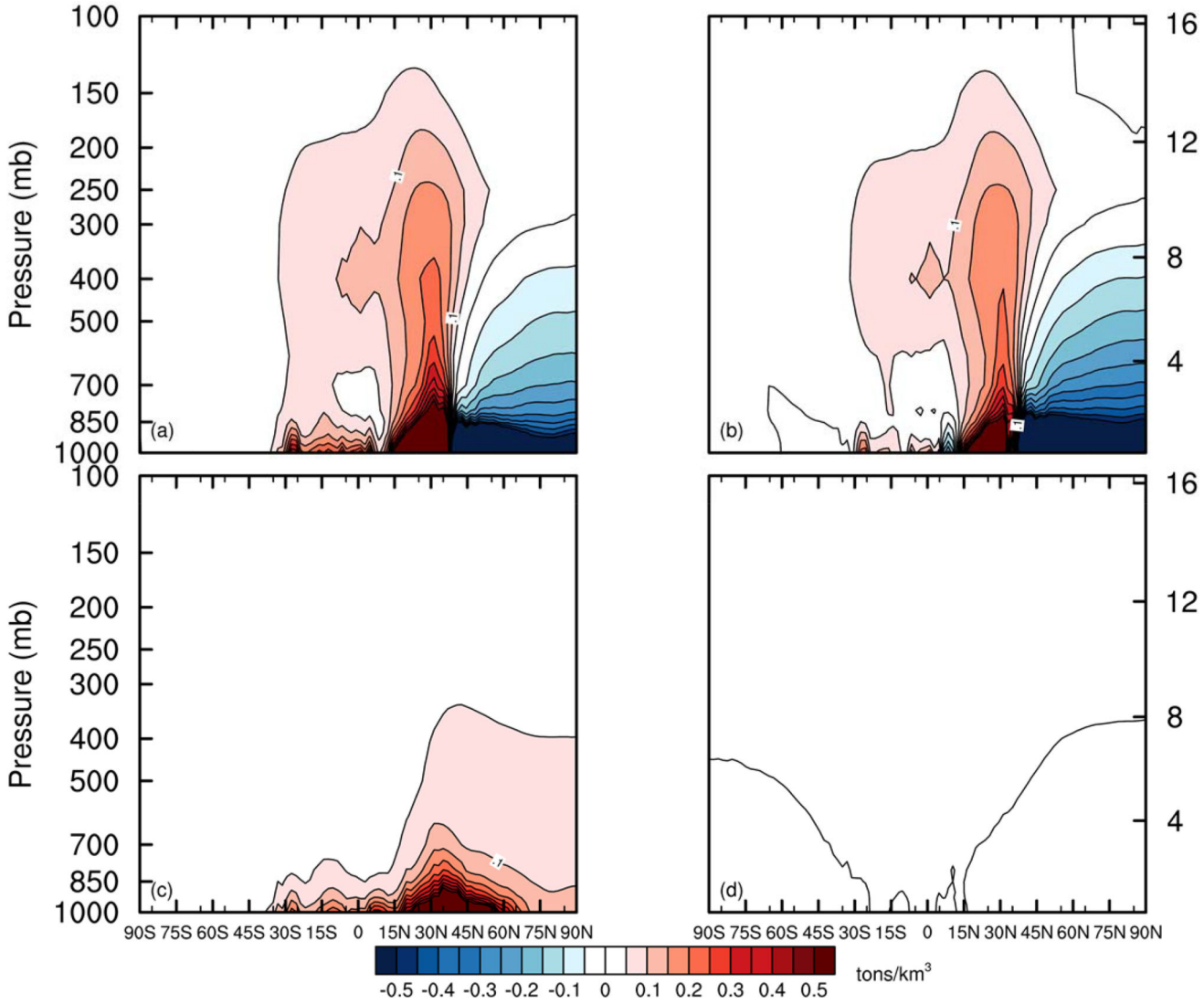

Figure 4. Zonal annual average NO_y change

a, Total changes from 1980 to 2010. **b-d,** Influences of changes in the global emissions spatial distribution, the global emissions magnitude, and global CH_4 mixing ratio. See Methods for the NO_y definition.